



**Institute for Theoretical  
and Experimental Physics**

**11-03**

ITEP-11-03

A. Akindinov, G. Bondarenko, V. Golovin,  
E. Grigoriev, D. Mal'kevich, A. Martemyanov,  
A. Smiritsky, K. Voloshin

LIBRARY

FEB 6 2004

**LIBRARY**

**Avalanche Photodiodes in the Geiger Mode  
for Scintillator Light Detection**

**M o s c o w**

**2003**

---

AVALANCHE PHOTODIODES IN THE GEIGER MODE FOR SCINTILLATOR LIGHT DETECTION: Preprint ITEP 11-03/

A. Akindinov<sup>\*1</sup>, G. Bondarenko<sup>2</sup>, V. Golovin<sup>3</sup>, E. Grigoriev<sup>4</sup>, D. Mal'kevich<sup>1</sup>, A. Martemyanov<sup>1</sup>, A. Smiritsky<sup>1</sup>, K. Voloshin<sup>1</sup> — M., 2003 — 8 p.

Plates of an organic scintillating plastic BC408,  $50 \times 50 \times 5 \text{ mm}^3$ , with a wavelength-shifting (WLS) fiber Kuraray Y11, embedded in circular grooves inside the plastic, were used in combination with  $1 \text{ mm}^2$  avalanche photodiodes working in the Geiger mode (APDg, or MRS APD, or SiPM). Beam tests with minimum ionizing particles (MIP), performed at the ITEP synchrotron, have shown high detection efficiencies of about 13 photoelectrons/MIP.

Summarized advantages of APDg — compactness, low operating voltage, high output signal, operation at room temperatures, low price, etc. — open wide possibilities in the construction of large area and low-cost scintillator detectors for calorimetry and active shielding. APDg characteristics compared to those of a standard photo-multiplier XP2020Q are presented.

А. Акиндинов, Г. Бондаренко, К. Волошин, В. Головин, Е. Григорьев,  
Д. Малькевич, А. Мартемьянов, А. Смирнитский

ЛАВИННЫЕ ФОТОДИОДЫ В ГЕЙГЕРОВСКОМ РЕЖИМЕ ДЛЯ РЕГИСТРАЦИИ СЦИНТИЛЛЯЦИОННОГО СВЕТА

Для задач светосбора в круглые канавки внутри пластин органического сцинтиллятора BC408 размером  $50 \times 50 \times 5 \text{ мм}^3$  помещалось оптическое волокно Kuraray Y11. Регистрация света осуществлялась лавинными фотодиодами диаметром 1 мм, работавшими в гейгеровском режиме (APDg, MRS APD или SiPM). Пучковые тесты с минимально-ионизирующими частицами (MIP), организованные на синхротроне ИТЭФ подтвердили высокую эффективность регистрации прибора, равную приблизительно 13 фотоэлектронов/MIP.

Сформулированные в статье достоинства APDg — компактность, низкое операционное напряжение, высокий уровень сигнала, работа при комнатных температурах, небольшая стоимость и т. д. — открывают широкие возможности использования прибора при создании больших по площади и недорогих сцинтилляционных детекторов для калориметрии и триггерных систем. Представлены основные характеристики APDg в сравнении со стандартным фотоумножителем XP2020Q.

Fig. — 11, ref. — 5 names.

© Институт теоретической и экспериментальной физики, 2003.

\* Corresponding author, e-mail: Alexandre.Akindinov@cern.ch.

<sup>1</sup> Institute for Theoretical and Experimental Physics, B.Chermushkinskaya 25, 117259, Moscow, Russia.

<sup>2</sup> Moscow Engineering and Physics Institute, Kashirskoe road 31, 115409, Moscow, Russia.

<sup>3</sup> Center of Perspective Technologies and Apparatus, Preobrazhenskaya sq. 6/68, 107076, Moscow, Russia.

<sup>4</sup> University of Geneva, CMU, Rue Michel-Servet 1, 1211 Geneva 4, Switzerland.

## 1. Introduction

An avalanche photo-diode (APD) seems to be a very promising device for various applications in the high energy physics. Despite high quantum efficiencies (Q.E.) for the visible light, currently known APDs (produced by HAMAMATSU) have rather low amplification coefficients. This turns to be the main disadvantage preventing one from creating fast electronics for sensitive light-detecting systems based on usual APDs.

A possible solution may be an APD operated in the Geiger mode (APDg). This device has an amplification coefficient of up to  $10^6$  (see Section 2.1), which facilitates the electronics creation, and widens the realm of the device employment.

APDg's have the Metal-Resistor-Semiconductor (MRS) intrinsic structure, and may be assembled in a micro-cell construction, as described in [1]. As it is known, such construction represents a lower Q.E. for the visible light, and a large photo-ionization coefficient (stipulated by cross-talks of 'red' photons between neighboring micro-cells), as explained in [2].

APDg's, which are described in this article, were designed and manufactured at CPTA<sup>3</sup>. They have satisfactory good Q.E. (20% in the green-yellow spectrum region) and comprise a special structure to suppress the photo-ionization.

Many possible applications of APDg are not mentioned in this article. The authors intend to use these devices in large low-light self-triggering systems working on cosmic rays, based on a 'tiles +

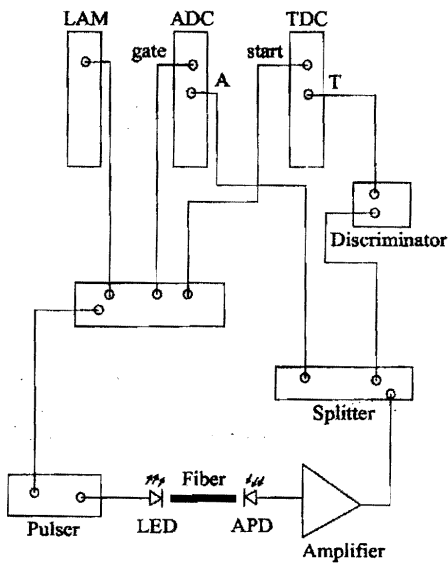


Fig. 1. Scheme of the laboratory setup used to test APDg.

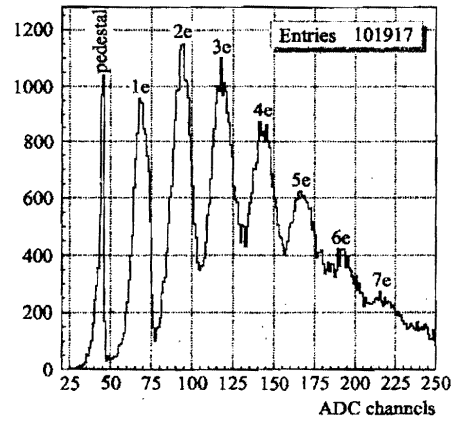


Fig. 2. Single electron spectrum from APDg obtained with low light pulses.

WLS fibers' architecture, and covering large surfaces.

## 2. Tests with LED

The laboratory setup, used to test new APDg's, is schematically shown in Fig. 1. The blue LED was put into work by a generated pulse, which had a triangle shape with an up to 5 V amplitude, a 5 ns rise-time, and a 15 ns fall-time. The light transmission was performed by KURARAY Y11 WLS fibers, 1 mm in diameter. The charge was measured with Le Croy QDC 2249 with a 50 ns gate, the time was measured with Le Croy TDC 2228. A tested APDg was placed inside a PVC optical connector to insure good coupling with the fiber. The connector itself was put into a screened copper box equipped with a VG3 amplifier, described in [3]. The main amplifier parameters were as follows: amplification — 0.9 V/pC, rise-time — 5 ns, fall-time — 8 ns, noise —

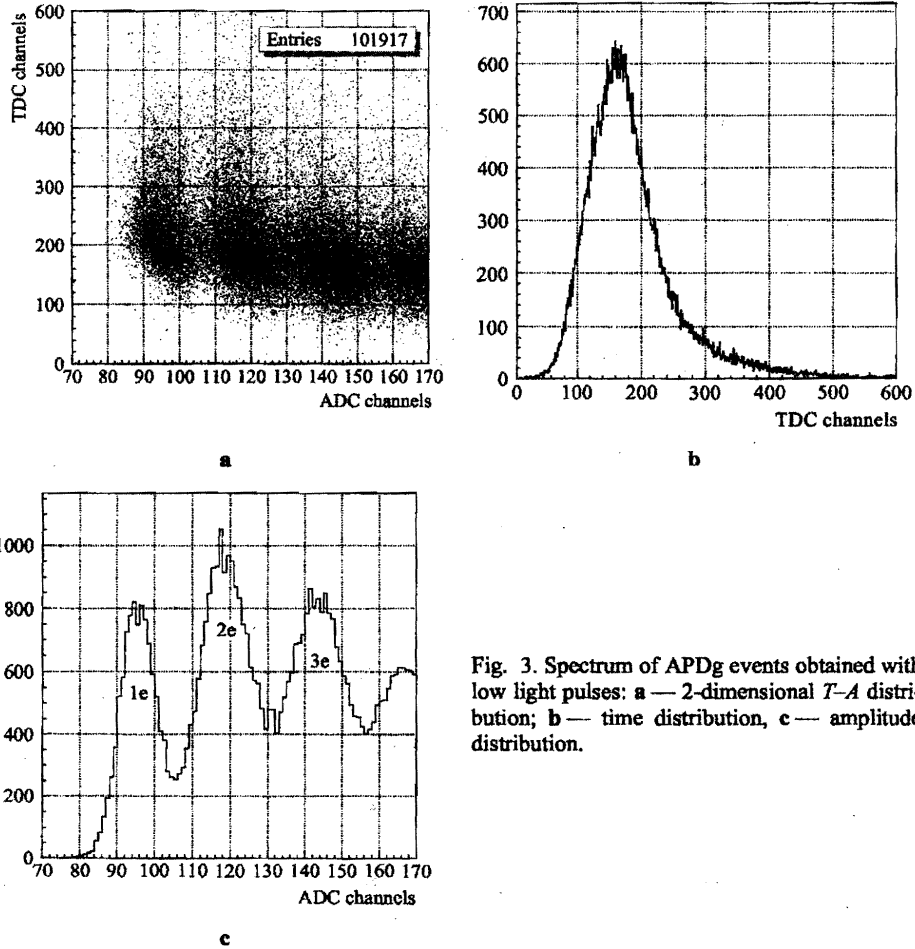


Fig. 3. Spectrum of APDg events obtained with low light pulses: a — 2-dimensional  $T$ - $A$  distribution; b — time distribution, c — amplitude distribution.

2500 e plus 60 e for every picofarade at the input.

Fig. 2 shows a single electron spectrum from APDg, obtained with low light pulses. Fig. 3 comprises a 2-dimensional  $T$ - $A$  distribution of the events measured with low light pulses, as well as its projections on the  $T$ - and  $A$ -axis. The amplitude spectrum represented in Fig. 3b was measured under an additional timing condition, insuring that the discriminator had snapped into action (within a 30 ns time window). Such spectrum gives a possibility to calibrate thresholds in terms of the number of photo-electrons.

### 2.1. Amplification

The APDg amplification depends on the applied voltage in a way represented in Fig. 4. Apart from the breakdown point, the curve looks linear with a 32% increase for each volt. Such slope corresponds to elementary micro-cell capacity  $\Delta Q/\Delta U$ . It may be seen that the amplification lies between  $10^5$  and  $10^6$ .

### 2.2. Noise Spectrum, Three Ways to Calculate the Number of Photo-Electrons

The upper plot in Fig. 5 shows a typical noise spectrum at  $U = 51.8$  V as a number of counts measured at different discriminating thresholds. Shown below in the same figure, is a corresponding self-triggering amplitude spectrum, in which one can see regions of 1, 2, 3, etc. electrons. With the lowest threshold, the count equaled to 1.2 MHz. It may be seen that increasing the threshold for a value corresponding to one electron leads to a fall of the count for approximately an order of magnitude.

The photo-ionization coefficient  $\alpha$  can be defined in a usual way as a probability to hit more than one cell with a single initial electron-hole pair:

$$\alpha = \frac{F_{n+1}}{F_n - F_{n+1}} = \frac{1}{10},$$

where  $F_n$  and  $F_{n+1}$  stand for the counts in the midles of the  $n$ -th and the  $(n+1)$ -th peaks correspond-

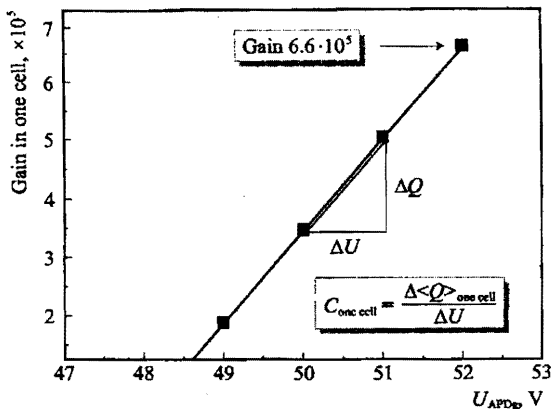


Fig. 4. APDg amplification as a function of the applied voltage. The slope corresponds to elementary micro-cell capacity  $\Delta Q/\Delta U$ .

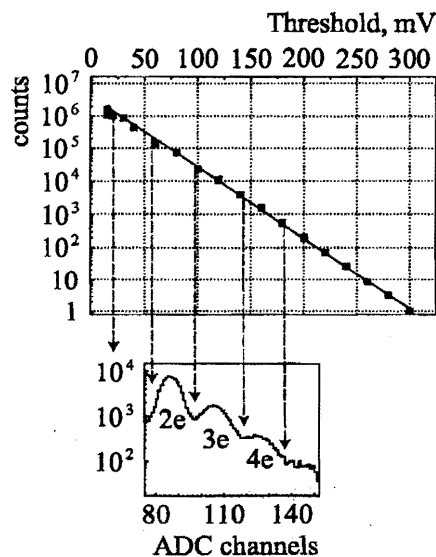


Fig. 5. Noise spectrum of APDg (above), and corresponding self-triggering amplitude spectrum (below).

ingly. The value of 1/10 is much better than that obtained with SiPMs (see [2]).

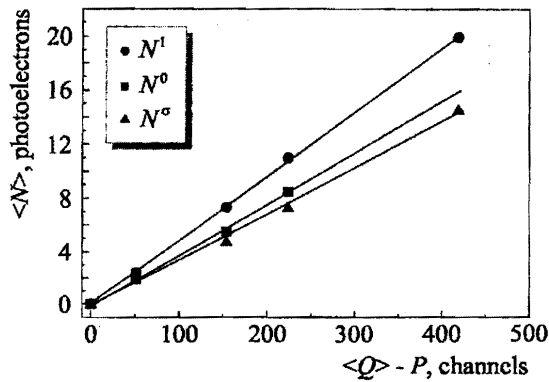


Fig. 6. Comparison of the three ways to estimate the number of photo-electrons in APDg. Explanation of the values is given in Section 2.2.

bution:

$$N^0 = -\ln P(0).$$

This estimation does not depend on the photo-ionization coefficient.

The lower curve shows the sigma estimation, the lowest one, which depends on the amplitude resolution:

$$N^\sigma = \left( \frac{\bar{Q} - P}{RMS} \right)^2.$$

The three estimations are related to each other in a way depending on the voltage:

$$N^1 = N^0 (1 + f(U_{APD})),$$

where  $f$  is the optical coupling coefficient. In case of  $U = 52.0$  V the above formula turns into the following relation:

$$N^1 = 1.32 \cdot N^0 = 1.45 \cdot N^\sigma.$$

This expression is important for the calculation of the number of photo-electrons exceeding 7 (when the amount of the events is small), or when the trigger is not 'clean' enough.

### 2.3. Choice of the Working Point

Fig. 7 shows a dependence of the noise spectrum on the applied voltage (Fig. 7a), and a curve describing a relative response of APDg to the Y11 WLS emission spectrum (Fig. 7b). Above 52.0 V, a plateau may be observed, while the noise continues to grow. To establish the best signal-to-noise ratio, a value of 51.8 V was chosen as the working point.

Fig. 6 illustrates three methods to calculate the number of photo-electrons.

The upper curve shows how the estimation may be performed basing on the amplitude of the first photo-electron peak:

$$N^1 = \frac{\bar{Q} - P}{\bar{Q}_{1e}},$$

where  $\bar{Q}$  is the average charge,  $P$  is the pedestal,  $\bar{Q}_{1e}$  is the most probable charge value from a single cell. This estimation appears to be the highest one, due to the photo-ionization.

The middle curve serves to make an estimation basing on the zero probability in the Poisson distribution:

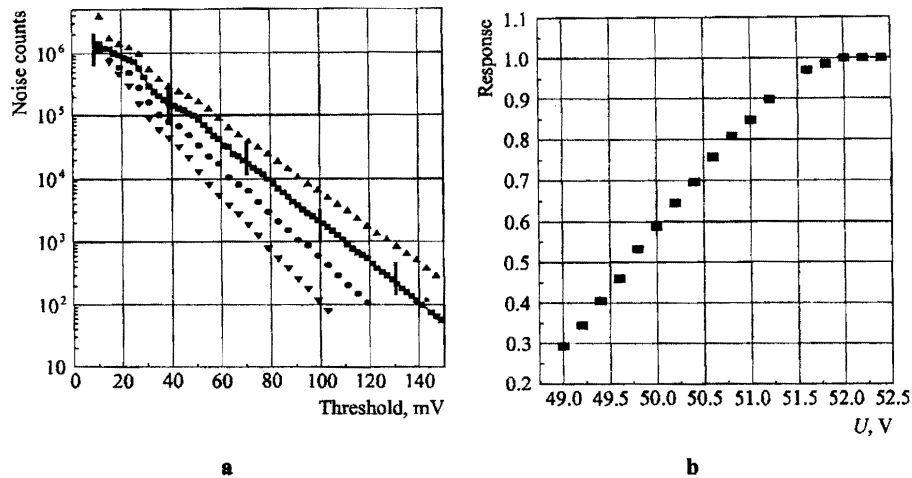


Fig. 7. Choose of the voltage working point: a — noise dependence on the threshold; b — APDg response to the Y11 WLS emission spectrum.

A detailed description of the APDg quantum efficiency, in comparison with the properties of a XP2020Q photo-multiplier, is set aside the main scope of this article, and may be found in Appendix.

### 3. Beam Tests of $50 \times 50 \text{ mm}^2$ Tiles

Beam tests were undertaken at the ALICE test beam facility at ITEP. The trigger was built of two big scintillator counters with  $150 \times 150 \times 10 \text{ mm}^3$  plastics, and of two smaller scintillator counters with  $50 \times 15 \times 10 \text{ mm}^3$  plastics, which were put in a cross-like position, and were equipped with mesh PMTs for timing measurements. TOF resolution of the start system equaled to 50 ps per counter. The average intensity of a 1.44 GeV/c  $\pi^-$ -beam was 4 kHz/cm<sup>2</sup>.

A tested tile was a  $50 \times 50 \times 5 \text{ mm}^3$  piece of scintillating plastic BC408 with a circular groove inside its body. 2 rings of Y11 WLS fiber, 1 mm in diameter, were inserted and glued into the groove. One end of the fiber was covered with aluminum, while the other, 0.5 m long and protruding from the tile, was left free for further connection to APDg. The tile was placed in the trigger center. The read-out scheme was left the same as during the tests with LED, except that the generator pulse was replaced with the coincidence of all the counters. The average APDg signal had a 10 ns rise-time and a 35 ns fall-time due to a distribution of light arrival times inside the tile.

A calibration spectrum for a low light is shown in Fig. 8a. The measurements were made directly at  $\pi^-$ -beam by taking the free end of the fiber 3 mm apart from the sensitive area of APDg. Figs. 8b and 8c represent  $T$  and  $T-A$  distributions correspondingly. The total width of the timing peak without  $T-A$  correction was about 25 ns. It may be seen in Fig. 8c that the discriminator threshold was set at the position of the 4-th photo-electron (corresponding to the 100-th channel in QDC). This led to the efficiency value of 99.3%. The noise count equaled to 1.2 kHz.

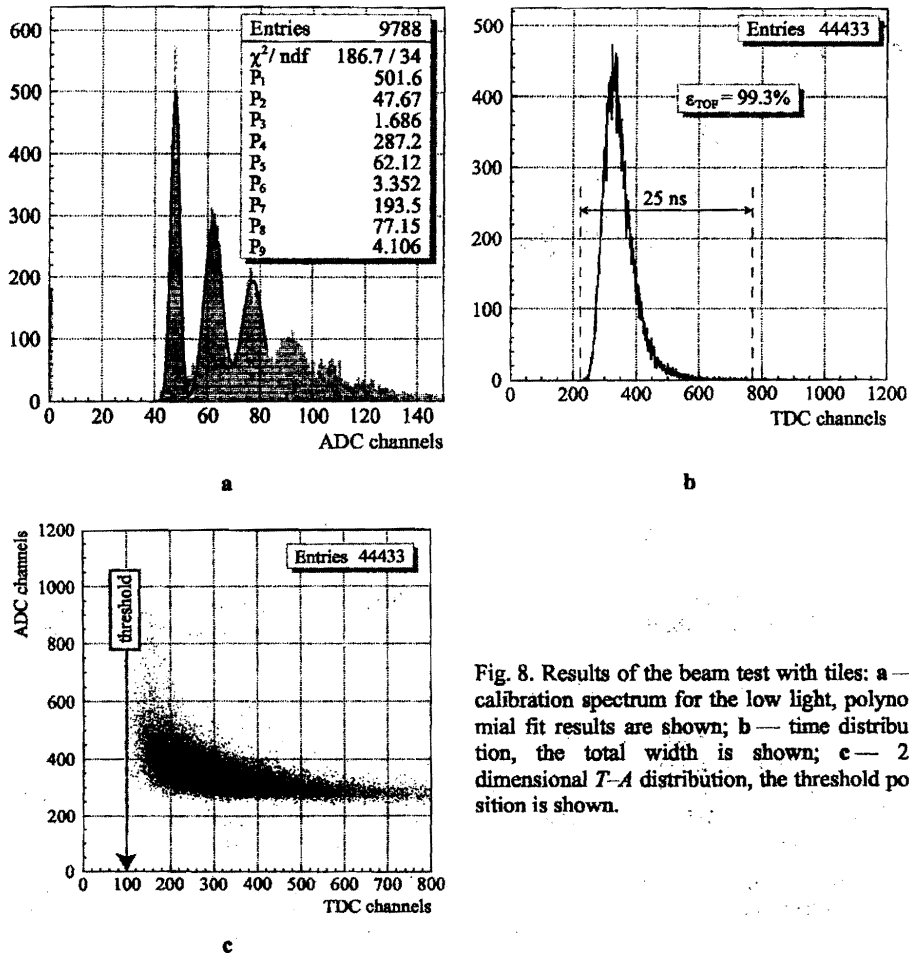


Fig. 8. Results of the beam test with tiles: a — calibration spectrum for the low light, polynomial fit results are shown; b — time distribution, the total width is shown; c — 2-dimensional  $T-A$  distribution, the threshold position is shown.

Fig. 9 compares amplitude spectra of APDg and PMT XP2020Q.  $N^\sigma$  and  $N^l$  were estimated by a gaussian fit of the left side of the Landau distribution, the right border of the fitting region being one sigma above the most probable value. Numbers of photo-electrons were determined as follows:

$$N^\sigma = \left( \frac{Q_{m,p}^{fit} - P}{\sigma^{fit}} \right)^2, \quad N^l = \frac{Q_{m,p}^{fit} - P}{Q_{le}}$$

The measurements resulted in  $N^\sigma = 12.9$  ph.e. and  $N^l = 14.7$  ph.e. for APD,  $N^\sigma = 10.5$  ph.e. for XP2020Q. One can see that in this case the relation between  $N^\sigma$  and  $N^l$  is slightly less than in case

of the LED tests, which is due to the fact that we use  $\sigma$  instead of R.M.S., and that the mean and the most probable values differ in the Poisson distribution.

#### 4. Conclusion

New APDg's, designed and manufactured at CPTA, have shown a high intrinsic amplification and a relatively low photo-ionization coefficient. The APDg Q.E. equals to 30–40%, which is comparable to that of standard photo-multipliers, and is shifted to the region of longer waves. In the Q.E. dependence on the applied high voltage, a plateau is present, which allows choosing the voltage by maximizing the signal-to-noise ratio. The use of Y7 and Y8 WLS fibers with a more 'green' spectrum will allow increasing the signal amplitude.

A low value of the photo-ionization coefficient makes it possible to use APDg by CPTA in cosmic-ray self-triggering systems. The next step will be a design of a  $150 \times 150 \times 10 \text{ mm}^3$  tile with two WLS fibers and two APDg's, which has been proposed as an essential part of the ALICE TOF (see [4]) Cosmic Ray Test Facility, aimed to test about 200 000 channels of Multi-Gap Resistive Plate Chambers, basic detectors for the ALICE TOF system, as described in [5].

#### Appendix.

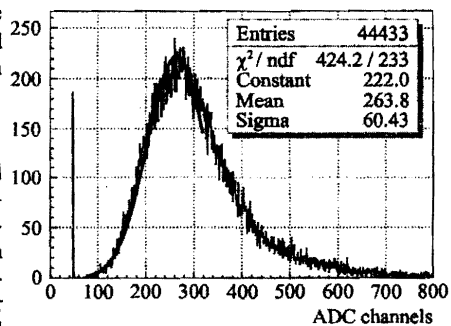
#### Quantum Efficiency of APDg in Comparison with PMT XP2020Q.

To compare Q.E. of APDg with that of a quartz-window photo-multiplier XP2020Q, special measurements of the amounts of photo-electrons have been performed. During the tests,  $1 \text{ mm}^2$  of sensitive surfaces of the both devices were irradiated with LEDs under identical conditions.

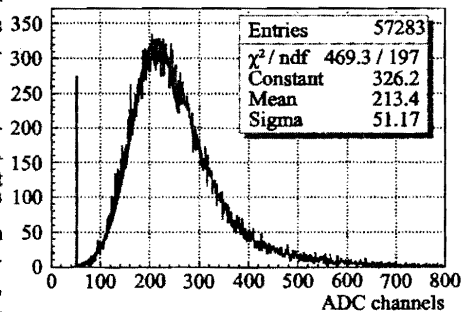
Fig. 10 shows charge spectra of APDg and XP2020Q in response to the light produced by three different LEDs with wavelengths of  $560 \pm 10 \text{ nm}$  ('yellow' region, Fig. 10a),  $520 \pm 10 \text{ nm}$  ('green' region, Fig. 10b), and  $470 \pm 10 \text{ nm}$  ('blue' region, Fig. 10c). To make the comparison clearer, the signals from APDg were magnified by a fast amplifier by about a factor of 100. This was done to make the mean values of the APDg and PMT amplitudes approximately the same.

In all the cases, the pedestals of the both devices were observed in same positions.

Despite close mean values of the APDg and PMT spectra, the distribution widths differed. The APDg width was approximately equal to that of PMT in the 'blue' part, while it turned significantly larger in the 'green' part, and even higher in the 'yellow' part.

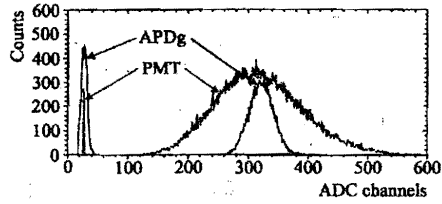


a

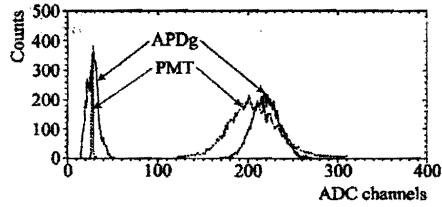


b

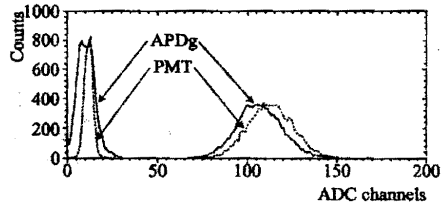
Fig. 9. Amplitude spectra of APDg (a) and PMT XP2020Q (b) measured under same conditions. The pedestal positions are shown with vertical bars.



a



b



c

Fig. 10. Amplitude distribution of signals from APDg and PMT XP2020Q, measured under identical conditions of irradiation with: a — yellow light,  $\lambda = 560$  nm; b — green light,  $\lambda = 520$  nm; c — blue light,  $\lambda = 470$  nm.

Quantitative results on the measurements of the APDg Q.E. are shown in Fig. 11. The estimations were based on a relation between the numbers of photo-electrons:

$$Q.E._{APDg} = Q.E._{PMT} \cdot \frac{N_{APD}}{N_{PMT}},$$

where  $Q.E._{PMT}$  is a well-known table value for PMT XP2020Q. Note that in the 'green' region, the Q.E. of APDg has been found to be as high as 35% or even more.

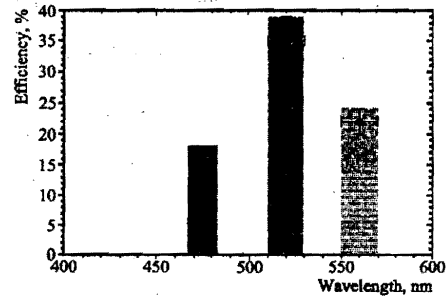


Fig. 11. Quantum efficiencies of APDg at different light regions.

### References

1. A. V. Akindinov, A. N. Martemianov, P. A. Polozov, et al., Nucl. Instrum. Methods A387 (1997), p. 231.  
V. Golovin, Patent of Russia # 1644708.
2. G. Bondarenko, B. Dolgoshein, V. Golovin, et al., Nucl. Phys. B 61B (1998), pp. 347–352.
3. A. Martemianov, WASA Memo, Uppsala, Sweden, 1994.
4. ALICE TOF Technical Design Report, CERN/LHCC 2000–12.
5. A. Akindinov, F. Anselmo, M. Basile et al., Nucl. Instrum. Methods A456 (2000), p. 16.